


Article

Experimental Study on Spray Cooling Heat Transfer of LN₂ for a Large Area

Jinhong Zhao ¹, Yanming Guo ¹, Qing Ai ^{1,*} , Jiaming Gong ^{1,2,*} and Yong Shuai ¹

¹ School of Energy Science and Engineering, Harbin Institute of Technology, Harbin 150001, China; guoyanming@hit.edu.cn (Y.G.)

² Institute of Industrial Science, The University of Tokyo, Tokyo 153-8505, Japan

* Correspondence: hitaiqing@hit.edu.cn (Q.A.); jiaming@iis.u-tokyo.ac.jp (J.G.)

Abstract: Spray cooling has been considered one of the most promising thermal control methods of high-heat flux devices. Most of the spray cooling research focuses on electronic components as the main application object to achieve higher heat dissipation heat flow in ambient temperature regions for small areas. Water is the most common cooling medium. This paper investigates the application of spray cooling thermal control over large areas. In this study, the heat-transfer characteristics of liquid nitrogen (LN₂) for large areas was investigated by conducting experiments. The test surface is 500 mm × 500 mm, which was cooled by a nine-nozzle array. The spray nozzles used in the experiment were conical nozzles with an orifice diameter of 1.6 mm, a spray angle of 120°, and a spray height of 42 mm. Liquid nitrogen was forcefully ejected from nozzles by the high pressure of a liquid storage tank to cool the test surface. According to the cooled surfaces, spray directions, and spray pressures, three groups of experiments were conducted. The results showed that the smooth flat surface has the best heat-transfer performance in three kinds of surface structures, which are macro surface, porous surface, and smooth flat surface. The heat-transfer coefficient varied by ±20% with different spray directions, and the surface heat-transfer coefficient increased linearly with increasing spray pressure. Most of the spray cooling research focuses on heat dissipation in the ambient temperature region for equipment over small areas. The results can benefit thermal control application in various fields. The research in this paper can provide a reference for the application of large-area spray cooling, and the application areas mainly include metal manufacturing processing cooling, aircraft skin infrared radiation characteristics modulation, and laser weapon equipment cooling.

Keywords: spray cooling; micro-grooved surface; porous surface; temperature control; liquid-nitrogen



Citation: Zhao, J.; Guo, Y.; Ai, Q.; Gong, J.; Shuai, Y. Experimental Study on Spray Cooling Heat Transfer of LN₂ for a Large Area. *Energies* **2023**, *16*, 3877. <https://doi.org/10.3390/en16093877>

Academic Editor: Antonio C.M. Sousa

Received: 9 March 2023

Revised: 16 April 2023

Accepted: 26 April 2023

Published: 3 May 2023



Copyright: © 2023 by the authors. Licensee MDPI, Basel, Switzerland. This article is an open access article distributed under the terms and conditions of the Creative Commons Attribution (CC BY) license (<https://creativecommons.org/licenses/by/4.0/>).

1. Introduction

Spray cooling has been widely used in various applications, such as multi-connected air-conditioning [1], power batteries [2], gas turbines [3], space and avionic devices [4], metal smelting, and processing industries [5]. The spray cooling heat-transfer characteristics have significant influence on heat-transfer performance, such as spray direction, spray pressure, surface modification, etc. Silk [4] studied the spray heat-transfer performance by using PF-5060; the spray inclination angle was 0°, 15°, 30°, and 45°, respectively. The inclined spray could effectively avoid the formation of the stagnation zone on the cooled surface, further improving the surface heat-transfer coefficient. Lou [6] experimentally studied the spray heat-transfer effect under low pressure and different spray angles. The larger the spray angle, the better was the heat-transfer effect, and when the spray angle increased by 15°, the temperature of the cooled surface decreased by about 0.5 °C. Liu [7] performed the spray cooling experiments by using water. It was found that an inclined spray could improve the heat-transfer coefficient and the coefficient reached the maximum value when the spray inclination angle was 18°. Compared with the heat-transfer coefficient

when the nozzle was not inclined, the coefficient increased by 20%. Gravity would affect the heat-transfer performance for different spray inclination angles. When the spray inclination angle was 0° , the droplet would spread on the surface under the action of gravity and surface tension while reaching the surface. It is easier to form a liquid film on the surface and expand the thermal area of phase transformation [8]. Spray pressure would affect the heat-transfer effect. Liu et al. [9] found that the heat flux of spray heat transfer increased significantly with the increase in spray pressure under the same superheat condition. A different spray flow rate provided a different heat sink, which led to a different heat-transfer performance. When the spray flow was greater than the surface evaporation, a liquid film would be formed on the surface, which increased the thermal resistance and reduced the heat-transfer coefficient. It was easy to form a local dry area on the surface while the spray flow rate was less than the evaporation and it achieved the highest heat-transfer coefficient when the spray flow rate was equal to the evaporation [10,11]. Surface modification is a way to enhance heat transfer. Jiang et al. [12] established the calculation model of a single nitrogen droplet impinging on different wetted wall surfaces and found that improving the wall wettability was beneficial to the radial diffusion of droplets which could increase the transfer area and improve the heat-transfer performance. Zhou et al. [13] experimentally studied the heat-transfer enhancement of modified surface in the closed-loop R404a flash spray cooling system. The surface with macro fins could tremendously enhance the heat transfer due to the increase in the wetted area. The nanoporous qualities could lead to better heat-transfer performance by increasing the number of nucleation sites and improving the wettability of the working fluid. Xu et al. [14] experimentally studied the heat-transfer performance of the spray on flat, rough, micro-structured, and hybrid micro-/nano-structured surfaces based on the R134a refrigeration cycle. Compared to the smooth surface, the micro-structured surface, rough surface, and hybrid micro-/nano structured surface could enhance the CHF by 42%, 15%, and 59%, respectively. In addition, the heat-transfer coefficient was also improved by 28%, 14%, and 42%, respectively. Opoku et al. [15] used deionized water spray cooling to investigate the spray heat-transfer performance of different surfaces. Both flat and wicking surfaces were investigated in experiments. The result showed that the modified wicking surface has a higher CHF of 225 W/cm^2 at the cooling temperature difference of 130°C compared to 160 W/cm^2 at the cooling temperature difference of 180°C . Li et al. [16] investigated the cooling performance of different surfaces using the gas-atomized water spray cooling system. It was found that hydraulic diameter of the micro-groove had a significant influence on the cooling performance of the gas-atomized spray cooling.

As shown in Table 1, most of the current research focuses on electronic components as the main application objects to achieve higher heat dissipation heat flow in small areas. Water is the most common cooling medium. In this paper, a spray cooling experimental system over a large area was designed and built, and liquid nitrogen was introduced as the working fluid. In an attempt to better investigate the enhancement effect of modified surfaces on spray heat transfer and further improving the heat-transfer performance of spray cooling, several experiments of different cooled surfaces, and different spray inclination angles and pressures, were carried out and discussed. The research in this paper can provide a reference for the application of large-area spray cooling, and the application areas mainly include metal manufacturing processing cooling, aircraft skin infrared radiation characteristics modulation, and laser weapon equipment cooling.

Table 1. Research of spray cooling.

Year	Application	Area of Cooling (mm ²)	Surface Nature	Spray Fluid
2006	Space and avionic device [4]	200	Flat surface	PF-5060
		400	Cubic pin fins	
		400	Straight fins	
2010	Electronic devices cooling [17]	450	Pyramids	Water
		30 × 30	Copper surface	
2013	Electronic devices cooling [18]	20 × 20	Flat surface	Water
2014	Electronic devices cooling [6]	7854	Micro-grooved surface	Water
			Stainless-steel surface	
2015	Electronic devices cooling [10]	113	Copper surface	R134a
			Al ₂ O ₃ -water-based nanofluid	
2015	Electronic devices cooling [19]	254	Copper surface	R134a
2017	Air-conditioning refrigeration and electronic devices cooling [11]	314	Copper surface	Water
2018	Airborne electronics cooling [8]	113	Micro-grooved surface	Water
2019	Spray cooling mechanism study [7]	408.9	Rectangular fins	Water
		361.8	Trapezoidal fins	
		316.2	Triangular fins	
		201.1	Projected area	
2019	Spray cooling mechanism study [12]	-	No-slip wall surface	Liquid nitrogen
2019	Electronic devices cooling [13]	177	Pyramid fins surface	R410a
			Square fins surface	
			Flat surface	
2019	Electronic devices cooling [20]	380 × 80	Nano-porous flat surface	Water
			Aluminum surface	
2019	Wind tunnel [21]	-	-	40% ethylene glycol aqueous solution
2020	Electronic devices cooling [14]	113	Flat surface	Liquid nitrogen
			Rough surface	
			Micro-structured surface	
2020	Electronic devices cooling [15]	-	Hybrid micro-/nano-engineered surface	Deionized water
			Smooth surface	
2021	Electronic devices cooling [9]	314	V-grooved surface	Water
2021	Electronic devices cooling [16]	13 × 13	Copper surface	Distilled water
2022	Air-conditioning refrigeration [1]	-	Micro-square fin surface	Water
			-	
2022	Battery cooling [2]	45 × 270	Aluminium surface	R134a
2022	Gas turbine [3]	-	-	Water
2022	Metal smelting and processing industry [5]	200 × 200	Steel surface	Water
2022	Thermal management [22]	148	Copper surface	Liquid nitrogen

2. Experimental Setup

The schematic of the experimental system is shown in Figure 1. The liquid-supplying system, heating system, and measuring system comprise the open-loop spray cooling system. Electric heating sheets and the voltage regulator are the main components of the heating system. The liquid-supplying system includes nozzles, the liquid storage tank, the solenoid valve, and the buffer tank. There is one inlet and nine outlets in the buffer tank, which can distribute the coolant from the liquid storage tank. The solenoid valve is controlled by the temperature controller. The temperature controller can regulate the temperature of the test surface by adjusting the flow of the working fluid through the solenoid valve. The thermocouples and the data-acquisition instrument in the measuring

system are the main instruments to monitor the temperature distribution of the test surface. The spray cooling experimental platform of LN2 is shown in Figure 2.

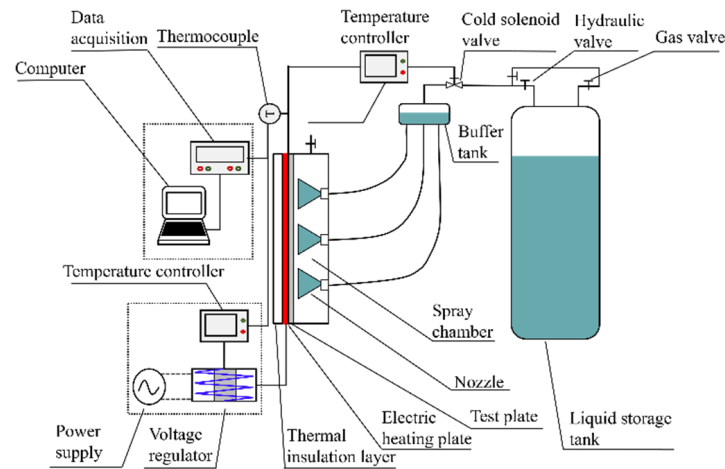


Figure 1. Schematic diagram of the experimental system.

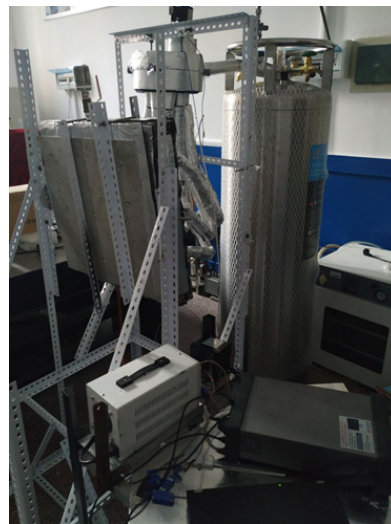


Figure 2. Experimental platform.

The experimental procedure is as follows:

- (1) Turn on the solenoid valve to keep the pipeline open, then pass nitrogen gas in the pipeline to discharge the air in the pipeline;
- (2) The initial temperature of the cooled surface is controlled at 20 °C by the electric heating sheet and the temperature controller. The opening and closing of the solenoid valve are controlled by another temperature controller, and the solenoid valve closes when the temperature of the cooled surface drops to −60 °C;
- (3) Turn on the data-acquisition instrument and detect the temperature data of the thermocouples. After initialization of the equipment is completed, open the regulator connected with the electric heating sheet so that the temperature of the cooled surface gradually rises and reaches stability. After the temperature of the cooled surface is stabilized for a period of time, close the regulator to stop the heating, and open the liquid supply valve so that the spray cooling system begins to work;
- (4) When the cooled surface temperature decreases to the set temperature, the solenoid valve automatically closes. As the surface temperature gradually rises, the temperature controller automatically adjusts the opening frequency and the duty cycle of the

- solenoid valve based on the temperature of the thermocouple and the set temperature to achieve the stability of the cooled surface temperature;
- (5) In the cooling process of the cooled surface, the temperature-change data of the temperature picking point on the back of the test plate is measured by the thermocouples with time, and the time taken for the temperature of the cooled surface to drop is displayed. The weighted average of the thermocouple test data is taken so that the cooling curve can be fitted. Then, the spray heat-transfer coefficients of the flat surface, micro-grooved surface, and porous surface can be calculated.

2.1. Spray System

The use of the nozzle array allows for better cooling performance in spray cooling compared to a single nozzle [23].

During the process of phase-change heat transfer, the governing equation is:

$$\frac{\partial(\rho\phi)}{\partial t} + \text{div}(\rho\mathbf{U}\phi) = \text{div}(\Gamma_{\phi}\text{grad}\phi) + S_{\phi} \quad (1)$$

Considering the convection and evaporation of each droplet and according to Equation (1), the heat balance equation is:

$$\frac{\partial(\rho\phi)}{\partial t} + \text{div}(\rho\mathbf{U}\phi) = \text{div}(\Gamma_{\phi}\text{grad}\phi) + S_{\phi} \quad (2)$$

The mathematical description of droplet evaporation is:

$$\frac{dm_d}{dt} = h_c A_d \rho_a \ln(1 + B_m) \quad (3)$$

The force balance equation of droplets under the influence of gravity and resistance in the movement is:

$$\frac{d\mathbf{u}_d}{dt} = F_D(\mathbf{u}_a - \mathbf{u}_d) + \frac{\mathbf{g}(\rho_d - \rho_a)}{\rho_d} \quad (4)$$

where F_D is a parameter relevant to the droplet, and F_D is defined as $F_D = \frac{18\mu}{\rho_d d_d^2} \frac{C_D \text{Re}_d}{24}$,

$$C_D = a_1 + \frac{a_2}{\text{Re}} + \frac{a_3}{\text{Re}^2}, \text{ and } \text{Re}_d = \frac{\rho_a d_d |\mathbf{u}_d - \mathbf{u}_a|}{\mu}.$$

According to Equation (1), the mass conservation equation is:

$$\text{div}(\rho_d \mathbf{u}_d) = \frac{dm_d}{dt} \quad (5)$$

Gong et al. [24] used a numerical simulation case to verify the appropriate distance of the nozzles in the nozzle array. In the simulation case, the effective cooling area of the test surface is 500×500 mm, and liquid nitrogen is used as the cooling medium. A conical nozzle is used in the numerical simulation case. The orifice diameter of the nozzle is 1.6 mm, and the spray diffusion angle is 120° . The distance between the nozzle and the test surface is 42 mm. The flow rate is 0.0228 kg/s. The cooling of the test surface was from the eighth second onwards. The whole process took 30 s and the heat flux is $16,000 \text{ W/m}^2$. Three different grid arrangements (3.53×10^5 , 1.72×10^6 , and 2.67×10^6 nodes) were examined. The temperature of the test surface was taken as the measuring standard and the grid size in the subsequent simulation was 1.72×10^6 . The numerical results of Gong et al. [24] are shown in Figure 3.

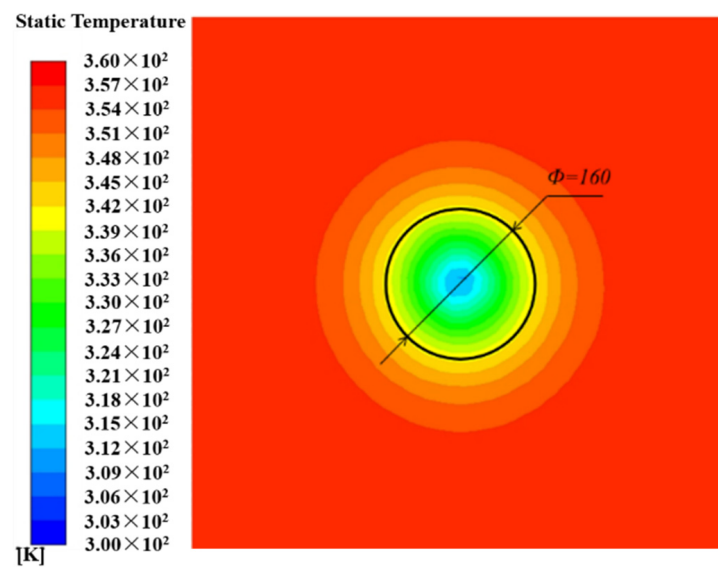


Figure 3. Temperature distribution of the test surface with a single nozzle in a steady state [24].

From Figure 3, it can be seen that in the test surface the temperature distribution is uniform and the effective zone of cooling for the single nozzle is a circular area with a diameter of 160 mm.

Based on the result of Gong et al. [24], the nozzle array should consist of nine nozzles, and the distance between each nozzle should be 166.66 mm, as shown in Figure 4. The characteristics of the nozzles used in the experiment are shown in Table 2.

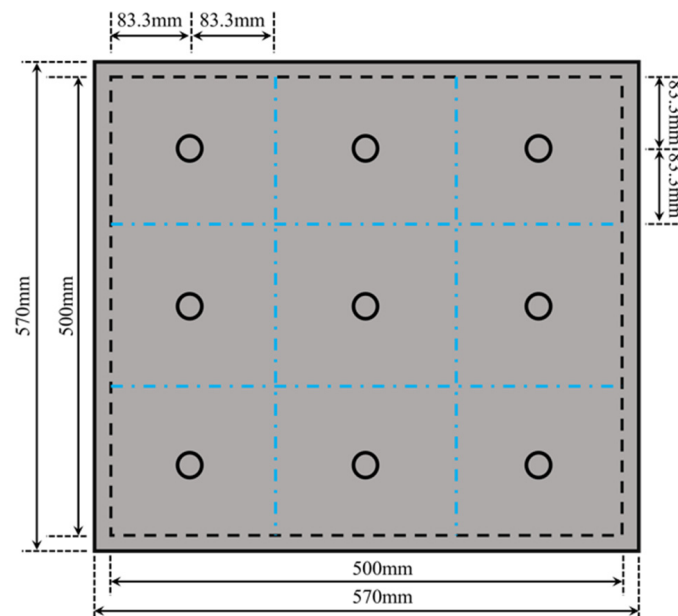


Figure 4. Nozzles layout.

Table 2. Characteristics of spray nozzles in the experiment.

Nozzle Type	Orifice Diameter (mm)	Spray Diffusion Angle (°)	Distance to Test Surface (mm)
Cone	1.6	120	42

2.2. Test Surface

Five different surfaces, including the micro-grooved surface and the test surface covered by porous foam, were investigated in this study. As shown in Figure 5, the smooth flat surface ($Ra < 0.25 \mu m$) is $570 \times 570 \times 3$ mm, constructed of 7075 aluminium, and the cooled area is 500×500 mm.

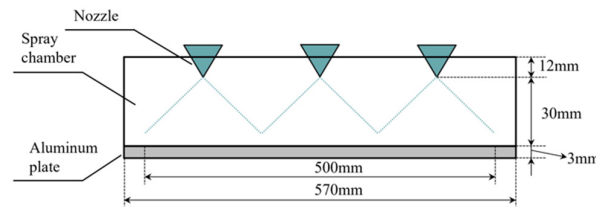


Figure 5. The smooth flat surface.

During the heat-transfer process of the aluminum plate, the surface heat-transfer coefficient could be described as [19]:

$$h = \frac{q}{T_w - T_d} \tag{6}$$

In this paper, the maximum heat power is 10 kW/m^2 , and the maximum between T_w and T_d is less than 100 K, and the maximum Biot number is:

$$Bi \leq \frac{\delta h}{\lambda} = 1.27 \times 10^{-3} \tag{7}$$

The Biot number is less than 0.1, and it can be considered that the internal temperature of the plate after cooling is not different. The differential equation of unsteady heat conduction in the aluminum plate can be simplified as:

$$\rho c V \frac{dT_w}{dt} = h A (T_d - T_w) \tag{8}$$

The surface heat-transfer coefficient can be obtained by integrating Equation (6):

$$h = \frac{\rho c V \Delta T_w}{A (T_d - T_w) \Delta t} = \frac{\rho c \delta}{(T_d - T_w)} \cdot \frac{\Delta T_w}{\Delta t} \tag{9}$$

The macro characteristics of the test surface with micro-grooves are shown in Figure 6. The size of the porous copper foam is $500 \text{ mm} \times 500 \text{ mm} \times 2$ mm. In this study, three kinds of porous copper foam with different porosities of 50 ppi, 80 ppi, and 110 ppi were selected. It can be seen from Figure 7 that the foam copper was covered on the smooth flat surface of the aluminum plate when it was in the experiment.

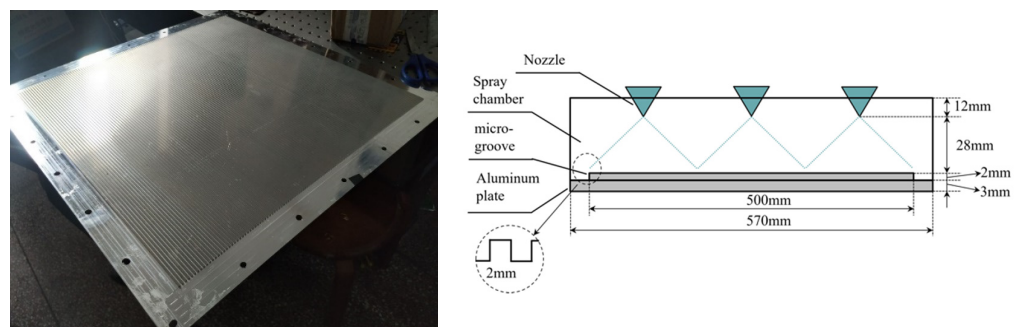


Figure 6. Test surface with micro-grooves.

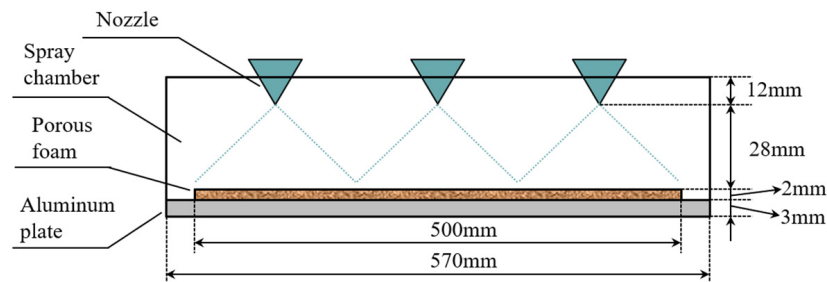


Figure 7. Schematic diagram of porous surface.

2.3. Heater Assembly and Experimental Measurement Facilities

An electric heating sheet was used for heating in the experiment and the heating power of the electric heating sheet is $0.1\sim 20\text{ kW/m}^2$. The electric heating sheet has a gelatinous layer attached to one side to hold tightly to the heated object and a 10 mm thick insulation layer to the other side to reduce the impact of the environment during the experiment.

During the experiment, the TT-T-36-SLE thermocouple manufactured by Omega company was used. The signals generated by the thermocouples were received in real time by Keysight DAQ970A and transmitted to the computer for processing.

3. Error Analysis

The external environment of the experimental system would cause bias in the experimental results. In the experimental process, the ambient temperature was higher than the cooled surface and the LN₂, and the external thermal environment would heat the cooled surface and the LN₂ flowing in the pipeline, resulting in heat loss in the experimental system. In addition, the cooled surface does not exist in isolation, and the supporting parts of the cooled surface would have an impact on the cooled surface temperature during the experiment. The temperature of the supporting parts would gradually drop during the experiment, and the temperature could reach a minimum of $11.6\text{ }^\circ\text{C}$. These factors would cause errors in the convective heat-transfer coefficient of the spray cooling.

In order to minimize heat loss, it was necessary to insulate each component. In this paper, foam polystyrene was used as the insulation material and each component was insulated using the stacking insulation method. The foam polystyrene thermal conductivity was $0.42\text{ W/(m}\cdot\text{K)}$. The relationship between the heat leakage and the insulation thickness is shown in Figure 8, and the thickness of the insulation layer used in the experiment was 30 mm.

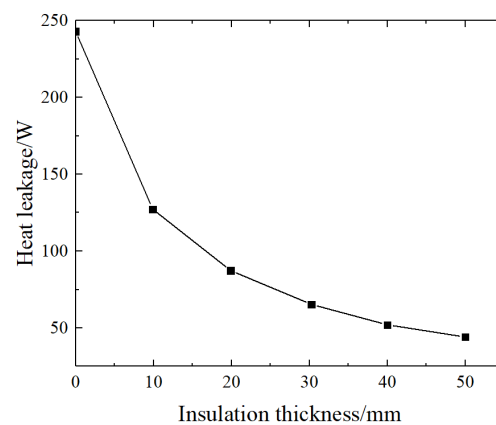


Figure 8. Change of unit heat exchange with insulation layer thickness.

In the experimental process, the outer surface of the electric heating sheet was covered by the insulation layer, and the heat would still be conducted within the insulation layer. The general heat loss was 2~3% of the total heat flux, which was $200\sim 300\text{ W/m}^2$.

The accuracy and scale range of the experimental equipment in the study is shown in Table 3.

Table 3. Parameters of experimental instruments.

Name	Scale Range	Error Range
TDGC2J voltage regulator	0~300 V	-
Electric heating sheet	~200 °C	±5%
Cold solenoid valve	~1.6 MPa	-
TT-T-36-SLE thermocouple	-200–260 °C	±0.4%
Data-acquisition instrument (Keysight DAQ970A)	-	0.004%

The electric heating sheet used in the experiment was heated by the electric heating wire and the surface heat source was of non-uniform temperature. The unevenness of temperature was ±3.6%. In this experiment, the density distribution of the spray droplets in different positions led to the inhomogeneity of the surface heat transfer and the difference of the surface temperatures. Multiple thermocouples were arranged on the surface to measure the temperature. The weighted average of the measured results was used to reduce the measurement error caused by the temperature inhomogeneity [17].

The heating power of the electric heater can be calculated by the voltage and resistance of the electric heater:

$$P = \frac{U^2}{R} \quad (10)$$

The uncertainty of the heating voltage measurement is ±0.5 V. The heat flux of the electric heater is:

$$q = \frac{U^2}{R \cdot S} \quad (11)$$

In order to study the uniformity of the cooled surface temperature, the *MSE* (mean square error) of temperature was analysed for the surface temperature measurement data. The calculation equation is [20]:

$$MSE = \sqrt{\frac{\sum_{i=1}^n (T_i - \bar{T})^2}{n(n-1)}} \quad (12)$$

The heat-transfer coefficient in the experiment was obtained by measuring the test surface temperature and its change rate. The error of the heat-transfer coefficient was calculated by using the Holman error transfer function [18]. The calculation formula is:

$$y = f(x_1, x_2, \dots, x_n) \quad (13)$$

$$Er_y = \sqrt{\left(\frac{\partial y}{\partial x_1}\right)^2 Er_{x_1}^2 + \left(\frac{\partial y}{\partial x_2}\right)^2 Er_{x_2}^2 + \dots + \left(\frac{\partial y}{\partial x_n}\right)^2 Er_{x_n}^2} \quad (14)$$

The rate of change of the surface temperature is:

$$\frac{\Delta T_w}{\Delta t} = f(T_w, t) = \frac{T_w' - T_w''}{t' - t''} \quad (15)$$

The error of surface temperature change rate is:

$$Er_{\frac{\Delta T_w}{\Delta t}} = \sqrt{2 \frac{1}{(t' - t'')^2} Er_{T_{At}}^2 + 2 \left[\frac{(T_w' - T_w'')}{(t' - t'')^2} \right]^2 Er_t^2} \quad (16)$$

Ignoring the time error, we can achieve:

$$Er_{\frac{\Delta T_w}{\Delta t}} = \sqrt{2 \frac{1}{(t' - t'')^2} Er_{T_w}^2} = \sqrt{2} \frac{Er_{T_w}}{t' - t''} \quad (17)$$

According to the relation of surface heat-transfer coefficient and error transfer function, we can achieve:

$$Er_h = \sqrt{\left(\frac{\rho c}{T_w - T_d} \cdot \frac{\Delta T_w}{\Delta t}\right)^2 \cdot Er_{\delta}^2 + \left(\frac{\rho c \delta \Delta T_w}{\Delta t}\right)^2 \cdot \left(\frac{1}{T_w - T_d}\right)^4 \cdot Er_{T_w}^2 + \left(\frac{\rho c \delta}{T_w - T_d}\right)^2 \cdot Er_{\frac{\Delta T_w}{\Delta t}}^2} \quad (18)$$

$$Er_h = \frac{\rho c}{T_w - T_d} \sqrt{\left(\frac{\Delta T_w}{\Delta t} \cdot Er_{\delta}\right)^2 + \left(\frac{\delta \Delta T_w}{\Delta t} \cdot \frac{Er_{T_w}}{(T_w - T_d)^2}\right)^2 + \left(\delta \cdot Er_{\frac{\Delta T_w}{\Delta t}}\right)^2} \quad (19)$$

According to Equations (18) and (19), the error of the surface heat-transfer coefficient is:

$$\begin{aligned} Er_h &= \frac{\rho c}{T_w - T_d} \sqrt{\left(\frac{\delta \Delta T_w}{\Delta t} \cdot \frac{Er_{T_w}}{(T_w - T_d)^2}\right)^2 + \left(\delta Er_{\frac{\Delta T_w}{\Delta t}}\right)^2} \\ &= \frac{\delta \rho c}{T_w - T_d} Er_{T_w} \sqrt{\left(\frac{\Delta T_w}{\Delta t (T_w - T_d)^2}\right)^2 + 2 \left(\frac{1}{t' - t''}\right)^2} \end{aligned} \quad (20)$$

When the surface temperature changes rapidly with time, the relative error of the surface heat-transfer coefficient is large. By substituting the temperature data and other parameter values into the above equation, the relative error of the surface heat-transfer coefficient in the experiment was about 4.86%.

4. Results and Discussion

4.1. The Effect of Different Surfaces on Cooling

Five different surfaces were selected, including the smooth flat surface ($Ra < 0.25 \mu\text{m}$), the micro-grooved surface, and three different copper-foam-covered surfaces. The cooling test was carried out on the five surfaces, which decreased from 303.05 K to 261.67 K. The heat power was 10 kW/m^2 .

The temperature in Figure 9 was the average temperature of the cooled surface. As can be seen from Figure 9, it took 36 s, 26 s, 40 s, 41 s, and 35 s for the temperatures of the smooth flat surface, micro-grooved surface, 50 ppi copper foam, 80 ppi copper foam, and 100 ppi copper foam to decrease from 303.05 K to 261.67 K.

The smooth flat surface could be rapidly cooled, and it maintained stability at low temperature. The surface was heated from 0 to 150 s to cause the temperature to rise near the specified temperature. 150 s to 500 s was the temperature-control process. 500 s to 700 s was the temperature-control process under the heat power of 10 kW/m^2 . Under the heat power of 10 kW/m^2 , the surface temperature could still be controlled at a low level, but the surface temperature varied greatly. After the temperature stabilized, the temperature of the central point was maintained at $253.57 \pm 0.69 \text{ K}$, and $255 \pm 0.78 \text{ K}$ at the far point. After adding 10 kW/m^2 heat power on the surface, the temperature of the central point was maintained at $245.47 \pm 9.21 \text{ K}$, and $258.89 \pm 4.5 \text{ K}$ at the far point. Stronger heat transfer of the spray at the center was achieved with dramatic temperature changes in the central area.

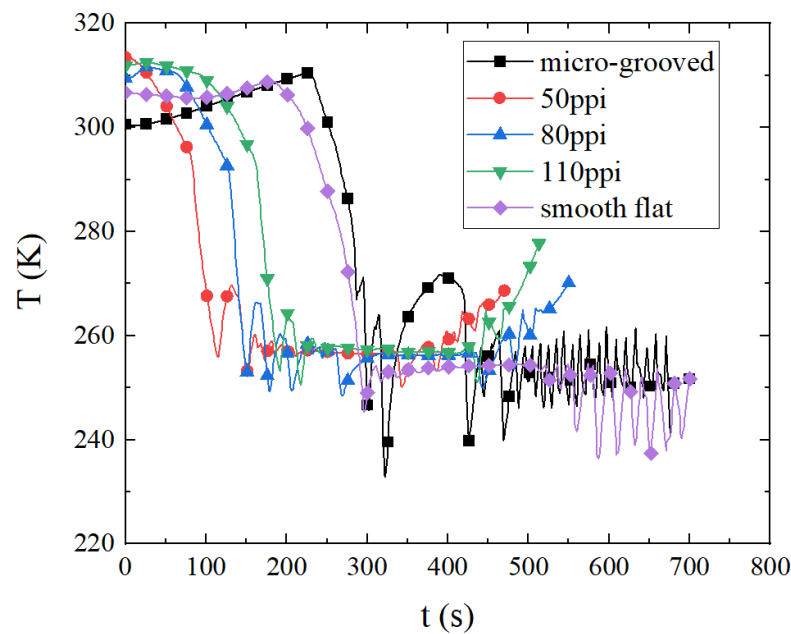


Figure 9. The cooling curve of different surfaces.

The temperature at the center point of the micro-grooved surface was maintained at 253.89 ± 7.76 K. The surface temperature fluctuation was slightly larger and the temperature far from the center could not be well controlled and the surface temperature would continue to rise, which indicated that the heat flux near the center point was higher than 10 kW/m^2 and the heat-transfer coefficient far from the center was lower. This may be because the macro-fins changed the surface flow field of the spray droplets. The droplets were more likely to flow to the channel between the macro-fins and drain out, resulting in the amount of retained droplets on the test surface being decreased and the surface heat-transfer coefficient being reduced. This showed that the micro-grooved surface could not achieve continuous temperature control under a high heat flux.

After the surface temperature was stabilized, the central temperature of the surface covered by the foam copper with a porosity of 50 ppi was maintained at 255.21 ± 0.79 K, and the distant temperature was maintained at 256.84 ± 0.31 K. After the surface temperature of the aluminum sheet covered with foam copper with porosity of 80 ppi was stabilized, the central temperature was maintained at 256.35 ± 0.33 K, and the distant temperature was maintained at 256.07 ± 0.72 K. After the surface temperature was stabilized, the central temperature of the surface covered by 110 ppi foam copper was maintained at 255.51 ± 0.21 K, and the distant temperature was maintained at 256.87 ± 0.18 K. It could be seen that the surface temperature uniformity was significantly improved after the surface was covered with foam copper.

After adding 10 kW/m^2 heat power on the surface (50 ppi at 325 s, both 80 ppi, and 110 ppi at 420 s), the surface temperature could not be maintained at a stable rate and it continued to rise. This indicated that the heat flux of the surface was less than 10 kW/m^2 . This may be because the copper surface was covered with foam. The porous structure increased the heat-transfer area and the flow resistance increased. The droplets impacted the surface with reduced velocity, and part of the liquid nitrogen was vaporized in the process of permeation to the copper foam. The effect of the copper foam on the normal resistance of the spray droplets along the cooled surface was greater than the radial penetration and diffusion of the liquid nitrogen droplets along the cooled surface. The heat-transfer coefficient decreased correspondingly and continuous temperature control under the large heat flux could not be achieved.

By comparing the heat-transfer performance of different surfaces, it was found that all five surfaces could achieve the goal of rapid cooling, and the temperature-control response

time was less than 1 min. The heat-transfer coefficients of different surfaces are shown in Figure 10. It could be seen that the heat-transfer coefficients of the surface with micro-grooves were lowest, while the heat-transfer coefficients of the smooth flat surface and the surface covered with copper foam were similar. According to Figure 9, only the smooth flat surface could achieve the stability of low temperature control under the high heat flux. Therefore, the smooth flat surface was used in the subsequent experiments.

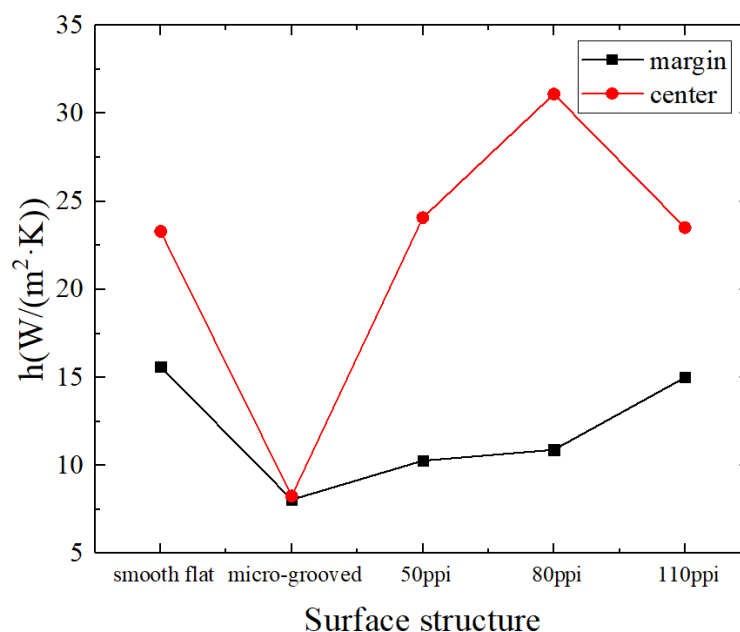


Figure 10. Average heat-transfer coefficients of the different surfaces.

4.2. The Effect of the Direction of Spray on Cooling

When the spray flowed vertically down to cool the horizontal surface, the droplets would spread outwards after reaching the surface and form a liquid film on the cooled surface under the action of the surface tension and strengthening the heat-transfer process. When the spray flowed along the horizontal direction to cool the vertically placed test plate, the droplets would flow downwards under the influence of gravity after reaching the surface, resulting in the instability of the liquid film formed in the cooled area. When the spray flowed vertically upwards to cool the test plate placed horizontally, the droplets reached the surface and were more likely to form droplets and sputter under the action of gravity (Figure 11). The spray cooling system may have different cooling effects under different spray directions (Figure 12). Therefore, the spray heat-transfer effect when the spray chamber was placed at different angles was considered for study (Figure 13).

The center temperature is the average temperature of T1, T2, T3, T4, T5, T6, T7, T8, and T9 in Figure 14, and the margin temperature is the average temperature of t1, t2, t3, and t4 in Figure 14.

The heat-transfer coefficient was higher in the central area than in the margin area. The heat-transfer coefficient was $103.34 \pm 4.34 \text{ W}/(\text{m}^2 \cdot \text{K})$ in the vertical downward spray, $86.28 \pm 9.13 \text{ W}/(\text{m}^2 \cdot \text{K})$ in the horizontal spray, and $65.7 \pm 5.86 \text{ W}/(\text{m}^2 \cdot \text{K})$ in the vertical upward spray. The results showed that the surface heat-transfer coefficient was significantly lower when spraying upward at the spray pressure of $0.4 \times 10^6 \text{ Pa}$, and the change of the heat-transfer coefficient was about $\pm 20\%$ when spraying in different directions. It can be seen that gravity had a great impact on the heat-transfer coefficient of spray.

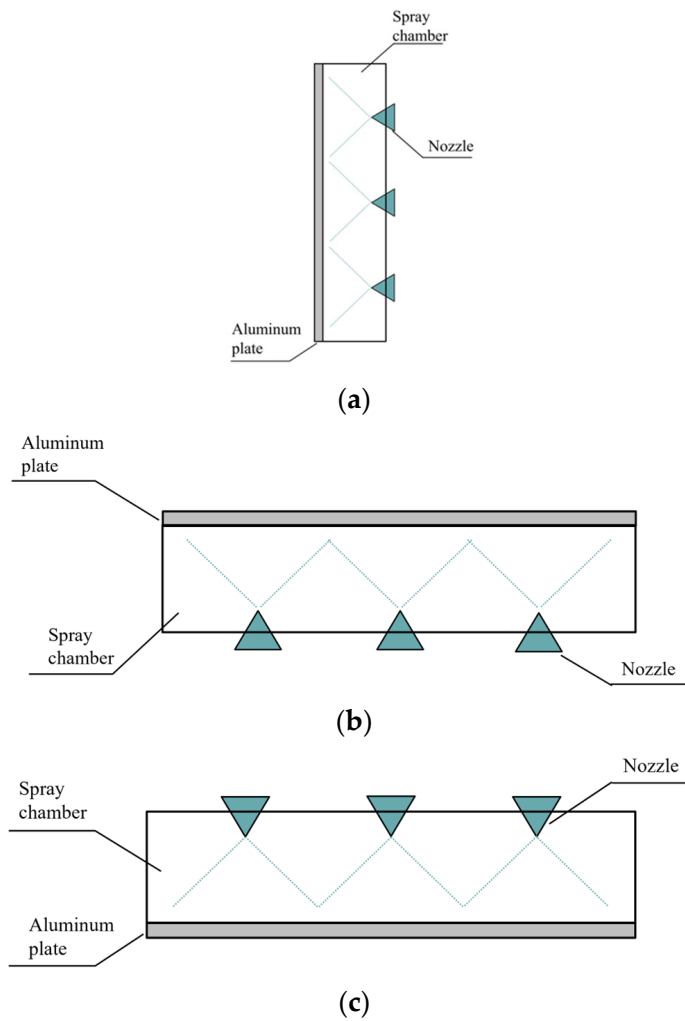


Figure 11. Schematic of different spray directions. (a) Horizontal spray; (b) vertical up spray; and (c) vertical down spray.

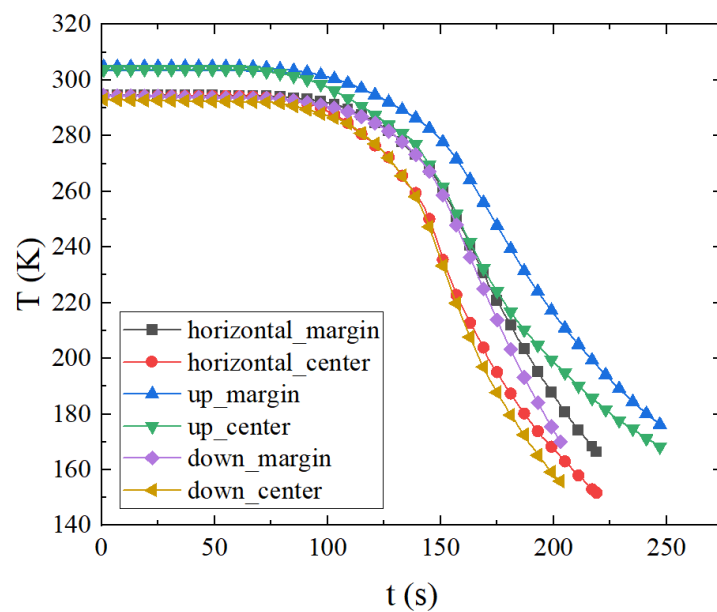


Figure 12. Temperature curve with time under different spray directions.

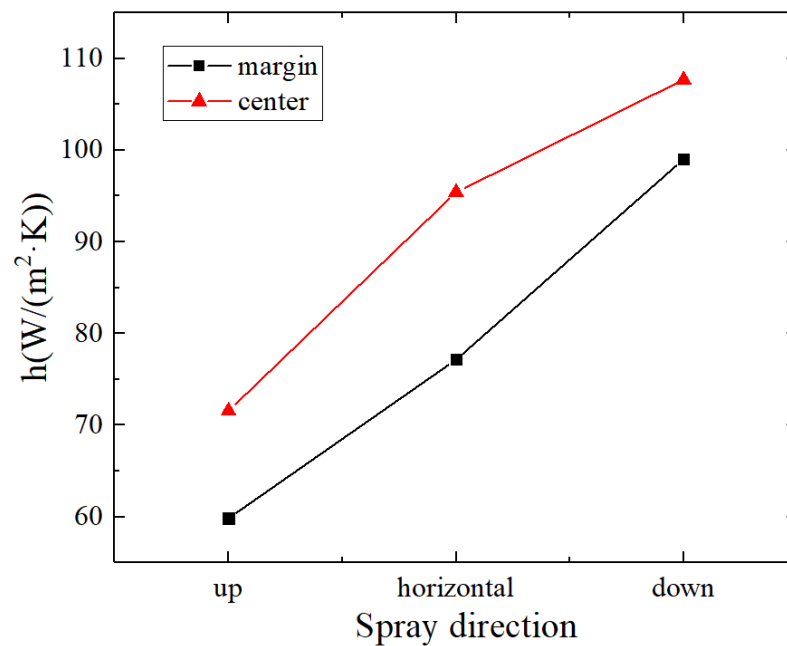


Figure 13. The heat-transfer coefficient under different spray directions.

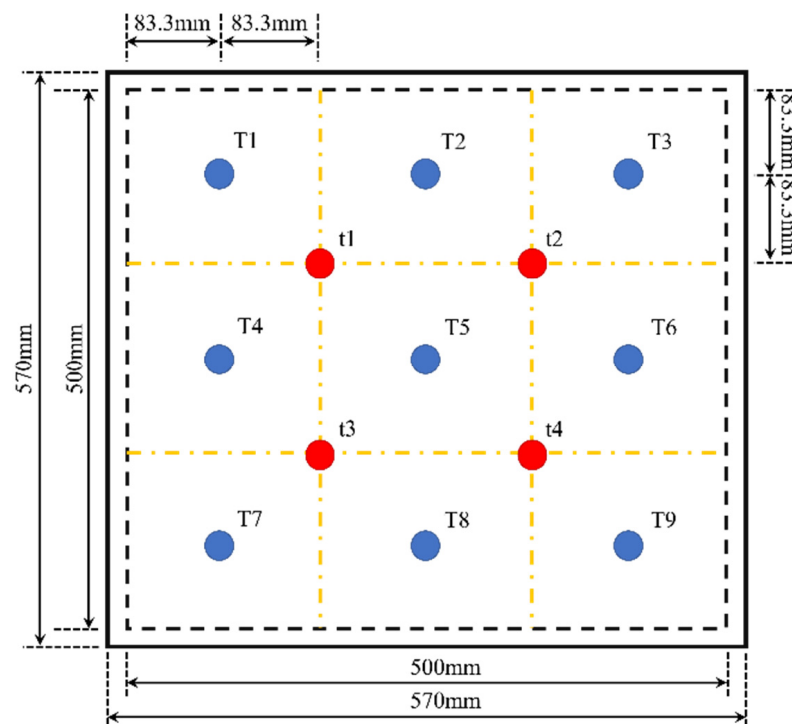


Figure 14. Arrangement of the thermocouples.

4.3. The Effect of Pressure on Cooling

It can be seen from Figure 15 that increasing the pressure could increase the surface cooling rate. When the spray pressure was 10^5 Pa, the surface heat-transfer coefficient was 24.22 ± 0.78 W/(m²·K); when the spray pressure was 2×10^5 Pa, the surface heat-transfer coefficient was 38.99 ± 2.84 W/(m²·K); and when the spray pressure was 4×10^5 Pa, the surface heat-transfer coefficient was 66.25 ± 6.72 W/(m²·K).

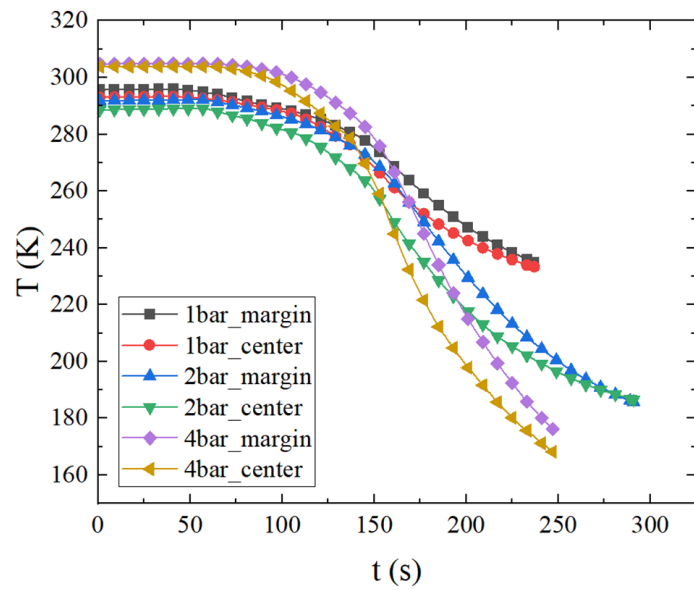


Figure 15. Temperature changes under different pressures in the vertical upward spray.

As can be seen from Figure 16, the greater the spray pressure, the greater the surface temperature drop of the test plate. As shown in Figures 17 and 18, the surface heat-transfer coefficient increased with the increase in the spray pressure and the heat-transfer coefficient of the surface increased at a higher rate with the increase in pressure when the spray was sprayed downwards. When the spray pressure was 10^5 Pa, the surface heat-transfer coefficient was 17.7 ± 6.64 W/(m²·K); when the spray pressure was 2×10^5 Pa, the surface heat-transfer coefficient was 49.66 ± 2.67 W/(m²·K); and when the spray pressure was 4×10^5 Pa, the surface heat-transfer coefficient was 103.54 ± 2.7 W/(m²·K).

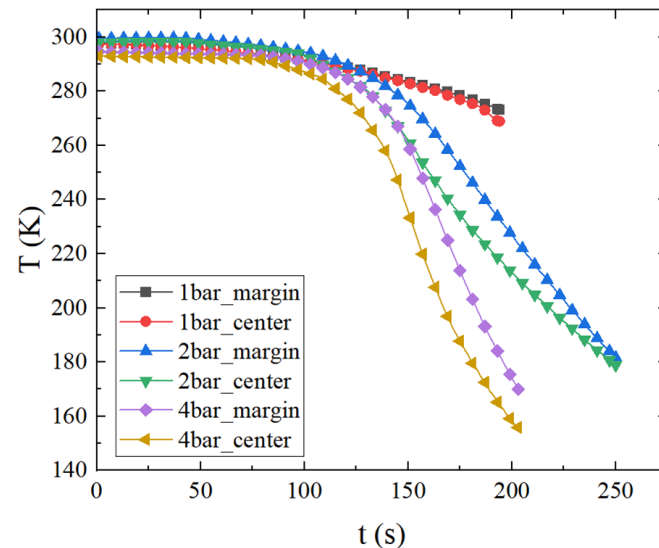


Figure 16. Temperature changes under different pressures in the vertical downward spray.

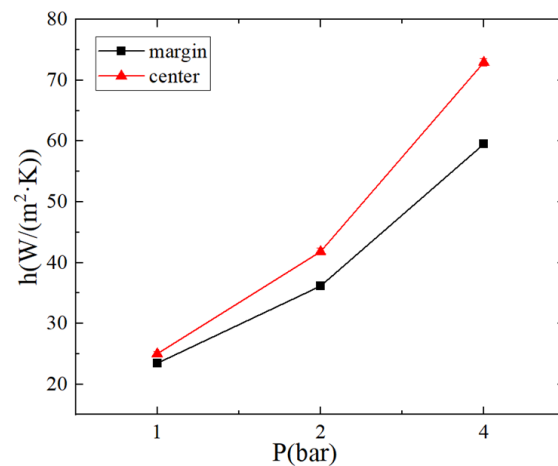


Figure 17. The heat-transfer coefficient under different pressures in the vertical upward spray.

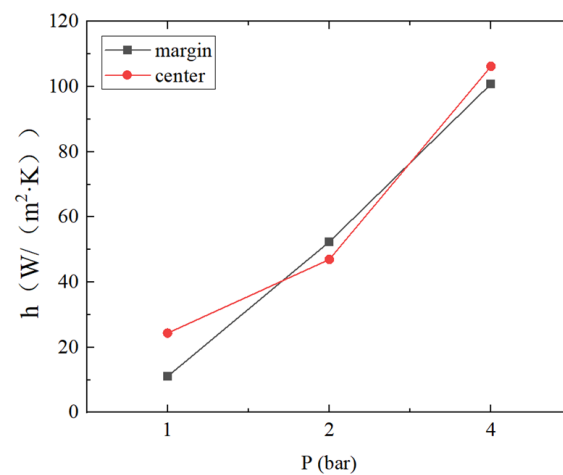


Figure 18. The heat-transfer coefficient under different pressures in the vertical downward spray.

5. Conclusions

With the continuous improvement of the detection ability of the infrared imaging system, the aerodynamic heating of the aircraft skin can be detected between 200 K and 350 K. While using coating materials to reduce the surface incidence and achieve infrared stealth, thermal environment control measures are adopted to cool the surface so as to reduce the infrared radiation intensity of the surface. Liquid nitrogen spray heat exchange, as a new rapid cooling technology, has the advantages of a fast cooling speed and a short response time, and is one of the effective ways to solve the problem of rapid large-scale cooling in a low-temperature environment.

In this paper, an experimental platform of LN₂ for large-area spray cooling was established. The spray heat-transfer characteristics of different cooled surfaces, and different spray directions and pressures were investigated. The following conclusions were obtained:

1. Five surfaces could achieve the goal of rapid cooling and a temperature-control reaction time of less than 1 min, but only the smooth flat surface could achieve the stability of low temperature control under high heat flux. In this paper, the enhanced heat-transfer effects of five different surfaces were compared. The experimental results showed that the enhanced heat-transfer effect of the smooth flat surface was the best, and the low temperature-control function could still be realized under the large heat power of 10 kW/m²;
2. In the experiment which studied the influence of spray direction, the heat-transfer coefficient was about 103.34 ± 4.34 W/(m²·K) when spraying vertically downward,

and $86.28 \pm 9.13 \text{ W}/(\text{m}^2 \cdot \text{K})$ when spraying horizontally. When spraying vertically upward, the heat-transfer coefficient was about $65.7 \pm 5.86 \text{ W}/(\text{m}^2 \cdot \text{K})$. The results showed that the surface heat-transfer coefficient was significantly lower when spraying upward at $4 \times 10^5 \text{ Pa}$, and the change of heat-transfer coefficient was about $\pm 20\%$ when the spraying direction was different. It could be seen that gravity had a great influence on the heat-transfer coefficient of the spray;

3. With the increase in the surface spray pressure, the surface heat-transfer coefficient increased. The results showed that the surface spray strengthening of the heat-transfer coefficient increases linearly along with the change of pressure, but the increased rate under a different spray direction was different, and, when spraying down, the surface heat-transfer coefficient with the increase in the pressure rate was higher.

Author Contributions: Conceptualization, Q.A., J.G. and Y.S.; Methodology, J.G.; Validation, Y.G.; Formal analysis, Q.A.; Investigation, J.Z. and Y.G.; Resources, J.G.; Data curation, J.Z. and Y.G.; Writing—original draft, J.Z.; Writing—review & editing, Q.A.; Supervision, Q.A. and Y.S.; Project administration, Y.S.; Funding acquisition, Y.S. All authors have read and agreed to the published version of the manuscript.

Funding: This work was supported by the National Major Scientific Instruments and Equipment Development Project of the National Natural Science Foundation of China (NSFC) (no. 52227813) and the National Key R&D Program of China (no. 2022YFC2204300).

Data Availability Statement: Public databases.

Conflicts of Interest: The authors declare no conflict of interest.

Nomenclature

\mathbf{U}	speed vector
S_g	generalized source term
m_d	quality of droplet
T_d	droplet temperature
T_a	temperature of environment
h_c	convection heat-transfer coefficient
h	surface heat-transfer coefficient
t	time
L_h	droplet evaporation coefficient
A_d	droplet surface area
B_m	mass exchange coefficient
F_D	drag coefficient
\mathbf{u}_d	velocity of droplet
\mathbf{u}_a	velocity of environment fluid
\mathbf{g}	gravity acceleration
Re	Reynolds number
Re_d	Reynolds number of droplet
q	heat flux
Bi	Biot number
T_w	temperature of the test surface
c	specific heat capacity of the test plate
P	heating power of the electric heater
R	resistance of the electric heater
S	heat area of the electric heater
T_i	measurement temperature of thermocouples
\bar{T}	average of the measurement temperature of thermocouples
$Er_{\frac{\Delta T_w}{\Delta t}}$	error of surface temperature change rate
Er_t	error of time

Er_h	error of the surface heat-transfer coefficient
Er_δ	error of the test thickness
Greek Letters	
ϕ	common variable
Γ_ϕ	generalized diffusion coefficient
ρ	variable density
ρ_a	environment fluid density
ρ_d	droplet density
δ	test plate thickness

References

1. Yalong, T. Application of Spray Cooling Technology in Multi-connected Air Conditioning (Heat Pump) Units. *Mod. Ind. Econ. Inf.* **2022**, *12*, 115–117.
2. Dong, B.; Sun, Q.; Gao, C.; Liang, K.; Li, Y.; Wang, L. Study on Spray Cooling Heat Transfer Performance of Power Battery. *J. Eng. Thermophys-Rus.* **2022**, *43*, 1588–1595.
3. Niu, C.; Hua, J.; Wang, K.; Liu, Z. Numerical Investigation on Flow and Heat Transfer in Spray Cooling of Gas Turbines. *J. Eng. Therm. Energy Power* **2022**, *37*, 91–96+194.
4. Silk, E.A.; Kim, J.; Kiger, K. Spray cooling of enhanced surfaces: Impact of structured surface geometry and spray axis inclination. *Int. J. Heat Mass Tran.* **2006**, *49*, 4910–4920. [[CrossRef](#)]
5. Hu, C. Online Local Enhanced Cooling and Property Control of Hot Rolled H-Beam. Master's Thesis, Yanshan University, Qinhuangdao, China, 2022.
6. Lou, J. Experimental Measurements and Theoretical Analysis Spray Cooling under Low Pressure. Master's Thesis, Harbin Institute of Technology, Harbin, China, 2014.
7. Liu, N.; Li, L.; Kang, Y.T. Experimental study on heat transfer performance enhancement by micro-structured surfaces for inclination spray application. *Int. J. Heat Mass Tran.* **2019**, *133*, 631–640. [[CrossRef](#)]
8. Long, H. Experimental Study on Heat Transfer Enhancement for Spray Cooling. Ph.D. Thesis, Nanjing University of Aeronautics and Astronautics, Nanjing, China, 2018.
9. Liu, L.; Wang, X.; Ge, M.; Zhao, Y. Experimental study on heat transfer and power consumption of low-pressure spray cooling. *Appl. Therm. Eng.* **2021**, *184*, 116253. [[CrossRef](#)]
10. Chunchao, Q. Investigation on Heat Performance of Spray Cooling System. Master's Thesis, Zhongyuan University of Technology, Zhengzhou, China, 2015.
11. Ranran, Y. Experimental and Theoretical Study on Spray Cooling to Enhance Heat Transfer. Master's Thesis, Hebei University of Technology, Tianjin, China, 2017.
12. Zhao, K.; She, Y.; Jiang, Y.; Qin, J.; Zhang, Z. Numerical study on phase change behavior of liquid nitrogen droplets impinging on solid surface. *Acta Phys. Sin.* **2019**, *68*, 244401. [[CrossRef](#)]
13. Zhou, Z.; Lin, Y.; Tang, H.; Fang, Y.; Chen, B.; Wang, Y. Heat transfer enhancement due to surface modification in the close-loop R410A flash evaporation spray cooling. *Int. J. Heat Mass Tran.* **2019**, *139*, 1047–1055. [[CrossRef](#)]
14. Xu, R.; Cao, L.; Wang, G.; Chen, J.; Jiang, P. Experimental investigation of closed loop spray cooling with micro- and hybrid micro-/nano-engineered surfaces. *Appl. Therm. Eng.* **2020**, *180*, 115697. [[CrossRef](#)]
15. Opoku, R.; Kizito, J.P. Experimental investigation of heat transfer characteristics and performance of smooth and wicking surfaces in spray cooling for high heat flux applications. *Results Eng.* **2020**, *6*, 100119. [[CrossRef](#)]
16. Wang, J.; Li, Y.; Zhong, M.; Zhang, H. Investigation on a gas-atomized spray cooling upon flat and micro-structured surfaces. *Int. J. Therm. Sci.* **2021**, *161*, 106751. [[CrossRef](#)]
17. Liang, Z. Design of Circulatory Spray Cooling System and Experimental Study of Spray Cooling. Master's Thesis, Xidian University, Xi'an, China, 2010.
18. Wei, Z. Investigation of Heat Transfer Characteristics of Spray Cooling on Micro-Grooved Surface. Ph.D. Thesis, China University of Petroleum (East China), Dongying, China, 2013.
19. Yang, Q.; Jionghui, L.; Mei, L.; Xiufang, L.; Yu, H. Experimental Study on Heat Transfer Performance of Phase Change Spray Cooling with R134a. *J. Xi'an Jiaotong Univ.* **2015**, *49*, 97–101.
20. Lijia, J. Study on Heat Transfer Characteristics of Compact Micro Spray Cold Plate. Master's Thesis, University of Science and Technology of China, Beijing, China, 2019.
21. Ruan, Y.; Hou, Y.; Xue, R.; Luo, G.; Zhu, K.; Liu, X.; Chen, L. Effects of operational parameters on liquid nitrogen spray cooling. *Appl. Therm. Eng.* **2019**, *146*, 85–91. [[CrossRef](#)]
22. She, Y.; Jiang, Y. Investigation on the spray cooling performance with liquid nitrogen. *Int. Commun. Heat Mass* **2022**, *136*, 106200. [[CrossRef](#)]

23. Hou, Y.; Tao, Y.; Huai, X.; Zou, Y.; Sun, D. Numerical simulation of multi-nozzle spray cooling heat transfer. *Int. J. Therm. Sci.* **2018**, *125*, 81–88. [[CrossRef](#)]
24. Gong, Y.; Zhao, J.; Li, W.; Ai, Q.; Gong, J.; Shuai, Y.; Sun, C. Experimental Investigation on Heat Transfer Characteristics of Liquid Nitrogen Spray Cooling for Large Area. *Energies* **2023**, *16*, 403. [[CrossRef](#)]

Disclaimer/Publisher’s Note: The statements, opinions and data contained in all publications are solely those of the individual author(s) and contributor(s) and not of MDPI and/or the editor(s). MDPI and/or the editor(s) disclaim responsibility for any injury to people or property resulting from any ideas, methods, instructions or products referred to in the content.